Bulletin of Engineering Geology and the Environment

Relation between crack initiation-damage stress thresholds and failure strength of intact rock

--Manuscript Draft--

Manuscript Number:	BOEG-D-17-00594R1
Full Title:	Relation between crack initiation-damage stress thresholds and failure strength of intact rock
Article Type:	Original Article
Corresponding Author:	Simone Mineo Universita degli Studi di Catania ITALY
Corresponding Author Secondary Information:	
Corresponding Author's Institution:	Universita degli Studi di Catania
Corresponding Author's Secondary Institution:	
First Author:	Giacomo Pepe
First Author Secondary Information:	
Order of Authors:	Giacomo Pepe
	Simone Mineo
	Giovanna Pappalardo
	Cevasco Andrea
Order of Authors Secondary Information:	
Funding Information:	
Abstract:	The analysis of a wide literature dataset of mechanical parameters related to intact rocks from more than 480 unconfined compression tests, coupled with new laboratory tests on 132 specimens, is proposed herein with the aim of analyzing the mechanical behavior of a great variety of rock types, mainly focusing on their crack initiation (ci) and crack damage (cd) stress levels. These thresholds can be employed as warning indicators for rock mass damage and breakouts and represent important input parameters for numerical models. International literature lacks in a detailed analysis on the mutual dependence existing between the main mechanical properties of intact rocks and their crack stress thresholds. In this paper, the study of the correlation between crack initiation-crack damage stress levels and the failure strength of sedimentary, metamorphic and igneous rocks is carried out through single and multiple regression approaches aimed at finding reliable prediction models, which can be useful when time-consuming laboratory experimental procedures need to be avoided. The correlation between predicted and measured values demonstrates that defined models represent a good tool for the empirical estimation of σci and σcd, and can be useful for preliminary engineering design dealing with stress-induced brittle fracturing, especially when the definition of warning indicators for rock mass damage and breakouts is needed. In fact, it is known that underground instability mainly depends on the redistribution of stresses around the excavation, which can produce induced stress concentrations, resulting in sudden release of stored energy and causing stress-induced brittle failure phenomena.
Response to Reviewers:	See attachment

Published in Bulletin of Engineering Geology and Environment on 16 October 2017 Volume 77 (2018) 709–724
https://doi.org/10.1007/s10064-017-1172-7

Relation between crack initiation-damage stress thresholds and failure strength of intact rock

Giacomo Pepe[1], Simone Mineo[2*], Giovanna Pappalardo[2], Andrea Cevasco[1]

[1] Department of Earth, Environmental and Life Sciences, Università degli studi di Genova, Corso Europa 26, 16132 Genova, Italy

[2] Department of Biological, Geological and Environmental Sciences, Università degli Studi di Catania, Corso Italia 57, 95129 Catania, Italy

*Corresponding author: Simone Mineo (smineo@unict.it)

Abstract

The analysis of a wide literature dataset of mechanical parameters related to intact rocks from more than 480 unconfined compression tests, coupled with new laboratory tests on 132 specimens, is proposed herein with the aim of analyzing the mechanical behavior of a great variety of rock types, mainly focusing on their crack initiation (σ_{ci}) and crack damage (σ_{cd}) stress levels. These thresholds can be employed as warning indicators for rock mass damage and breakouts and represent important input parameters for numerical models. International literature lacks in a detailed analysis on the mutual dependence existing between the main mechanical properties of intact rocks and their crack stress thresholds. In this paper, the study of the correlation between crack initiation-crack damage stress levels and the failure strength of sedimentary, metamorphic and igneous rocks is carried out through single and multiple regression approaches aimed at finding reliable prediction models, which can be useful when time-consuming laboratory experimental procedures need to be avoided. The correlation between predicted and measured values demonstrates that defined models represent a good tool for the empirical estimation of σ_{ci} and σ_{cd}, and can be useful for preliminary engineering design dealing with stress-induced brittle fracturing, especially when the definition of warning indicators for rock mass damage and breakouts is needed. In fact, it is known that underground instability mainly depends on the redistribution of stresses around the excavation, which can produce induced stress concentrations, resulting in sudden release of stored energy and causing stress-induced brittle failure phenomena.

Keywords: brittle failure, crack initiation stress, crack damage stress, crack propagation, lateral strain response, regression analysis, uniaxial compressive strength

1 Introduction

During underground excavations, damage and failures of the surrounding rock mass often give rise to stability problems that can affect the safety of the construction works. In case of highly stressed and massive rock volumes, where discontinuities do not play a significant role, underground instability mainly depends on the redistribution of stresses around the excavation. This can produce induced stress concentrations, which in turn may result in sudden release of stored energy, thus causing stress-induced brittle failure phenomena such as spalling, slabbing and bursting (Hoek et al. 1995, Hoek and Brown 1997). For massive to moderately jointed rock masses, in-situ strength is expected to be as close as possible to the laboratory measured uniaxial compressive strength (σ_{ucs}). However, in technical literature several cases of underground projects, along with in-situ experiments, showed that operational strength of rock masses can be significantly lower than the laboratory measured σ_{ucs}, depending also on the local geological setting, which affects the rock mass mechanical attitude (Pelli et al. 1991; Martin 1997; Read et al. 1998; Hajiabdolmajid and Kaiser 2003; Diederichs et al. 2004; Cai et al. 2004; Read 2004; Rojat et al. 2009; Cai and Kaiser 2014; Pappalardo 2015; Mineo et al., 2017).

Over the last decades, the detailed analysis of the uniaxial compression stress-strain response has proved to be very useful in understanding the in-situ rock mass strength (Martin et al. 1999; Diederichs 2007; Andersson and Martin 2009; Martin and Christiansson 2009). Several researchers dealt with the detailed quantification of stress-induced brittle fracture damage in rock (Hoek and Bieniawski 1965; Brace et al. 1966; Wawersik and Fairhurst 1970; Lajtai 1974; Tapponnier and Brace 1976; Stacey 1981; Huang et al. 1993; Martin and Chandler 1994; Eberhardt et al. 1998; 1999a; Nicksiar and Martin 2012). Their studies suggested that crack initiation (σ_{ci}) and crack damage (σ_{cd}) stresses could be used as warning indicators for rock mass damage and breakouts (Damjanac and Fairhurst 2010). More recently, extensive studies examined σ_{ci} and σ_{cd} quantities in various intact rock types (i.e. rock with no joints or hair cracks, after Terzaghi, 1946) highlighting that some conflicting views still exist about the reliability of universal stress levels defining rock damage stages under uniaxial compression (Hidalgo and Nordlund 2013; Nicksiar and Martin 2013; Xue et al. 2014). As other mechanical properties of natural geomaterials, also σ_{ci} and σ_{cd} seem to be affected by a certain variability (Nicksiar and Martin 2014). At the microscale, rocks are heterogeneous media made up of mineral aggregates together with defects such as pores, cracks and grain boundaries that, overall, contribute in causing scattering and variability in their mechanical properties. It is well known that variability is unavoidable in soil and rock mechanical characterization and it can result from many sources of uncertainties (Phoon and Kulhawy 1999; Sari and Karpuz 2006; Prakoso and Kulhawy 2011; Bedi and Harrison 2013; Pappalardo et al. 2013; Pappalardo and Mineo 2016; Pepe et al. 2017). Furthermore, the methods proposed to establish the stress associated with crack development are usually time-consuming and require detailed

laboratory tests with accurate measure of strain, especially when σ_{ci} has to be evaluated. Namely, precise procedures are required and, based on the adopted method, a certain degree of uncertainty and subjectivity is expected (Eberhardt et al. 1998; Nicksiar and Martin 2012). International literature lacks in a detailed statistical analysis on the correlations between the main mechanical properties of intact rocks and their crack stress thresholds. Therefore, this paper aims at evaluating statistical models for predicting σ_{ci} and σ_{cd} from single and multiple regression analyses. To this purpose, an extensive dataset was compiled with the main mechanical parameters of 483 specimens of igneous, sedimentary and metamorphic rocks, retrieved from international literature. Collected data were statistically analysed to highlight their variability and to study the mutual dependence between their main mechanical parameters. In particular, single and multiple regression analyses were performed by taking into account available data and the most satisfactory trends were considered to extrapolate suitable equations to predict σ_{ci} and σ_{cd}. Subsequently, achieved equations were validated through a comparison between predicted and measured values of 132 rock specimens properly tested herein through uniaxial compression tests. Measured crack stress thresholds and peak values were considered as a reference in order to establish the reliability of provided equations.

2 Overview on intact rock deformation processes under compression

2.1 Stress-induced brittle fracture damage

According to the earlier researches on rock deformation processes, it is widely accepted that the stress-strain response under uniaxial compression can be split into five stages (Fig. 1): i) crack closure; ii) linear-elastic deformation; iii) crack initiation and stable crack growth, iv) crack damage and unstable crack growth; v) failure and post-failure behaviour. Experimental evidences demonstrated that the transition from one stage to the next can be identified by the following stress thresholds (Fig. 1): crack closure stress (σ_{cc}), crack initiation stress (σ_{ci}), crack damage stress (σ_{cd}) and uniaxial compressive strength (σ_{ucs}). During the initial step of the loading path, the closure of pre-existing voids occurs. As a result, the stress-strain response is non-linear showing an upward concave shape of the axial stain curve, reflecting a gradual increase in the axial stiffness. By further increasing the applied axial stress, the rock damage process is characterized by the onset of new cracks. Microscopic investigations on laboratory-fractured rock specimens showed that the new microcracks initiate at the ends of pre-existing flaws when the tensile strength of the material is exceeded (Hoek and Bieniawski 1965; Lajtai 1998; Perras and Diederichs 2014). Such microcracks are mostly oriented parallel to the applied load and their growth is considered a stable process, which means that fracture propagation is slow and can be stopped by controlling the applied load. Once developed, cracks grow both in size and quantity and begin to interact each other. Accordingly, damage propagation will continue and fractures coalescence occurs until the crack damage stress is attained. Beyond this critical point, cracks propagation cannot be controlled by the operator, thus becoming an unstable process. Eventually, when the peak strength is reached, the tested specimen will be affected by macroscopic failures generally aligned with the maximum principal stress.

2.2 Crack stress thresholds detection

Crack closure stress (σ_{cc}) indicates the point where a linear elastic deformation takes place since the pre-existing defects can be considered all virtually closed (Fig. 1). Although it is generally accepted that the crack damage stress threshold can be detected at the point where the total volumetric strain (ε_v) reversal occurs, the evaluation of the crack initiation stress threshold has some critical aspects. A review of the procedures proposed in literature for the evaluation of the crack initiation stress was reported by Nicksiar and Martin (2012), who differentiated between volumetric and lateral strain methods (Fig. 2). The former can be further distinguished according to the volumetric strain adopted in establishing the onset of crack initiation. When the total volumetric strain is used (Fig. 2a), σ_{ci} is localized where ε_v departs from linearity

(Brace et al. 1966; Bieniawski 1967). Conversely, Martin and Chandler (1994) suggested that a better indicator for crack initiation is the crack volumetric strain (ε_{cr}), which quantifies the increase in volumetric strain due to the opening of new cracks and can be calculated by subtracting the elastic volumetric strain (ε_{el}) from the total volumetric strain (Fig. 2b). As stated above, since under compressive loading cracks tend to develop perpendicular to the least principal stress, lateral strain is considered as one of the most sensitive strain in detecting the initiation of new cracks (Lajtai 1974; Stacey 1981). Consequently, several authors suggested to localize the onset of crack initiation either where lateral strain departs from linearity (Fig. 2c) or through the detection of changes in the ratio of the lateral strain to axial stress (Fig. 2d). Diederichs (2007) proposed that σ_{ci} could be determined using a plot of the average tangent Poisson's ratio versus the log of the axial stress (Fig. 2e).

The greater amount of the proposed methodologies can suffer from user judgment, particularly if the tested specimen is affected by numerous pre-existing flaws. On the one hand, defects can influence the determination of the elastic parameters needed for the elastic volumetric strain assessment; on the other hand, they can cause a non-linear response of lateral strain for the entire test duration. Acoustic emission (AE) monitoring techniques were also coupled with strain monitoring to improve crack initiation (Fig. 2f) and damage stress levels recognition (Eberhardt et al. 1998). However, some difficulties can still affect the precise differentiation between background noise and acoustic events due to triggering of new microcracks. More recently, Nicksiar and Martin (2012) proposed a new procedure, called Lateral Strain Response (LSR) method, which removes the user judgment. This methodology (Fig. 3) relies on the assessment of the change in lateral strain (ΔLSR), which is defined as the difference between the recorded lateral strain and the linear lateral strain reference line. The reference line represents a theoretical linear lateral response between the zero stress and the point where unstable crack growth occurs. The crack initiation stress threshold is determined by plotting the change in lateral strain difference versus the axial stress and by fitting a polynomial equation to easily detect the stress associated with the maximum change in lateral strain. Such authors statistically demonstrated that the LSR method gives accurate results.

3 Materials and Methods

3.1 Literature data

A bibliographic dataset with results of 483 unconfined compression tests, carried out on intact rock specimens of sedimentary, igneous and metamorphic type, was compiled by means of an extensive research in literature (Table 1 and references therein). The attention was mainly focused on retrieving $\sigma_{ucs,}$ σ_{ci} and σ_{cd} values to be statistically treated, and intact rock stiffness properties (i.e. tangent Young's modulus and Poisson's ratio) when reported.

Several rock types were taken into account, thus providing a well-assorted and representative dataset in terms of mechanical behaviour. In fact, considered rocks vary from weak to extremely strong materials and show different mechanical attitudes under compression, resulting in a wide range of $\sigma_{ucs,}$ σ_{ci} and σ_{cd} (Fig. 4). In particular, minimum and maximum σ_{ucs} values are related to sedimentary and igneous specimens respectively, while intermediate values are found for metamorphic samples. Normalized values reveal that, on average, the onset of dilatancy occurs at about 46% of the peak strength, while unstable crack propagation stands around its 80%. This is a relevant aspect, highlighting that for about half of the available strength, rock specimens react to compression without being affected by cracking; on the other hand, crack damage is reached at the final stages of the test, thus controlling the failure pattern of the rock, which can be explained in terms of damage evolution and energy release (Pappalardo et al. 2016a). These preliminary considerations, in accordance with several studies carried out for rocks (e.g. Nicksiar and Martin 2013; Xue et al. 2014; Pepe et al. 2016) and for other classes of brittle materials (e.g. Contrafatto et al., 2016), support that σ_{ci}/σ_{ucs} and σ_{cd}/σ_{ucs} can be considered as intrinsic properties of rocks and could be used in rock engineering for predicting their failure processes.

3.2 Testing procedure

Besides the bibliographic dataset, new laboratory tests were carried out with the aim of both increasing the literature record and validating the prediction model presented in this paper. Experimental data were obtained from unconfined compression tests carried out on metamorphic and sedimentary intact rock specimens. In particular, metamorphic rock samples come from site investigation boreholes performed for a dam project in Ethiopia while sedimentary rocks were obtained from investigation cores drilled for some civil engineering projects in the Liguria Region (northwestern Italy). Cylindrical specimens were obtained from NQ (47.6 mm), HQ (63.5 mm) and PQ (85 mm) size cores. Specimens were carefully prepared according to the American Society for Testing Materials specification D4543-08 (ASTM 2001) in order to avoid both edge and size effects (Fig. 5). A length-diameter ratio (L/D) of 2.0 to2.3 was used to minimize the

shape effect (Thuro et al. 2001). Following ASTM requirements D2938-95 (ASTM 2001), unconfined compression tests were performed on 132 specimens in dry conditions using a servo-controlled testing machine (CONTROLS system with a stiff frame and a loading capacity of 3000 kN connected to the Advantest9 Computerised control console). The stiffness properties were evaluated conforming to the standard procedure ASTM D3148-96 (ASTM 2001). Tangent Young's module (E_{t50}) was calculated as the slope of a tangent to the stress-axial strain curve at a stress level equal to 50% of maximum load, while Poisson's ratio (ν_{t50}) as the ratio between the slope of lateral and axial strain curves at the same stress level. Crack initiation stress was evaluated adopting the Lateral Strain Response (LSR) method proposed by Nicksiar and Martin (2012). As stated before, the stress level σ_{cd} associated with the unstable crack growth was determined as the reversal point of total volumetric strain curve.

3.3 Experimental data

Experimental dataset consists of the main mechanical parameters of the following six rock types, tested according to the previous section: meta-leucogranite, meta-granite, meta-syenogranite, meta-granodiorite, meta-monzonite and limestone (Fig. 5b). The number of specimens tested for each rock type is summarized in Table 2, while a detailed description of the mineralogical and textural features of the metamorphic rocks can be found in literature (Pepe et al. 2016, 2017). In summary, meta-leucogranite, meta-granite, meta-syenogranite and meta-granodiorite essentially show high content of quartz, K-feldspar and plagioclase (Table 2). Conversely, quartz content is generally low in meta-monzonite, which on average contains higher percentages of femic minerals. Tested specimens show fine to medium grain size, massive structure and texture from weakly foliated to foliated. Limestones normally show homogeneous and massive texture and are mainly made up of calcite with negligible quartz and muscovite crystal fragments but with more or less abundant microfossils (Pepe et al. 2015). On average, all the tested specimens showed a low weathering degree.

The main experimental results are summarized in Table 3 and Figure 6, while the complete experimental dataset is given in Appendix A1. From the statistical point of view, sedimentary samples show narrower ranges if compared with metamorphic rocks. Average values of σ_{ucs} and E_{t50} reveal that metamorphic rocks are both stronger and stiffer than sedimentary samples. Average and standard deviation values of σ_{ucs} are 206.8 (±42.7) MPa and 121.4 (±28.6) MPa for metamorphic and sedimentary types, respectively. For metamorphic materials, Young's modulus is 59.9 (±8.2) GPa, while for sedimentary samples it is 41.0 (±13.5) GPa. According to the coefficient of variation, E_{t50} is far less variable in metamorphic rocks than in sedimentary ones. Conversely, it can be noted that the crack initiation and damage stress quantities exhibit similar degrees of variability among the two rock categories (Table 3). The coefficient of variation ranges from 24.9% to 26.0% for σ_{ci} and from 21.8% to 22.7% for σ_{cd}. The scatter is lower for the ratios σ_{ci}/σ_{ucs} and

σ_{cd}/σ_{ucs}. In fact, σ_{ci}/σ_{ucs} shows coefficient of variation varying between 15.2% and 16.3% while σ_{cd}/σ_{ucs} is in the range 6.7-9.4% (Table 3). Compared with the above reported literature dataset, experimental data collection of σ_{ucs}, σ_{ci} and σ_{cd} measurements used in this study is wider in terms of variety of rocks and number of specimens for each rock group. This aspect further strengthens the results of the statistical analysis commented herein.

3.4 Statistical analysis

With the aim of providing an alternative way to calculate σ_{ci} and σ_{cd} stress thresholds, whose estimation in laboratory requires strict procedures as above stated, a statistical analysis has been carried out on the dataset summarized in Table 1, through single and multiple regression approaches.

In particular, single regressions with confidence and prediction limits of 95% were carried out between unconfined compressive strength (σ_{ucs}), crack initiation stress (σ_{ci}), crack damage stress (σ_{cd}), Young's modulus (E_{t50}) and Poisson's ratio (ν_{t50}) by plotting variables against each other, in order to verify the possibility to predict one parameter from another. The equations of the best-fit curves and the coefficients of determination were calculated by the "least squares" method. Literature data were treated both as a single population, to obtain "general" prediction equations, and as different groups of rocks based on their origin process (i.e. igneous, metamorphic and sedimentary), to gain "particular" equations for each group of rocks. On the other hand, multiple regressions were aimed at achieving more specific equations to estimate crack initiation and damage stress quantities starting from two known variables. This kind of analysis is supported by correlation matrix and residual analysis, which prove the goodness of presented models.

Subsequently, achieved equations were employed for the empirical assessment of crack initiation and damage stress levels of rocks belonging to the experimental dataset. Such predicted values were correlated to the correspondent measured ones in order to highlight any differences and to validate proposed equations.

4 Results

4.1 Single regression analyses for general prediction equations

By considering the bibliographic database, the most satisfactory correlations refer to σ_{ucs}-σ_{ci} and σ_{ucs}-σ_{cd} (Fig. 7). In this case, two positive linear trends, with high coefficients of correlation ($r \geq 0.96$) and determination ($r^2 \geq 0.91$), *p*-value <0.001 and narrow confidence and prediction limits, are obtained. Such results highlight the goodness of treated data and allow making interesting considerations. Firstly, crack initiation and damage stresses are strongly dependent on the rock failure strength. Overall, as the peak strength increases, the quantity of stress needed to onset crack initiation and unstable crack propagation increases. These observations are consistent with the findings of previous works (Brace et al. 1966; Nicksiar and Martin 2013; Xue et al. 2014) reporting that, despite the wide range of rock origin process and the orders of magnitude range in peak strength values, a linear correlation seems to exist between crack stress thresholds (σ_{ci} and σ_{cd}) and σ_{ucs}. Therefore, universal stress levels defining the initiation of stable and unstable crack growth under compression could be reasonably assumed. Secondly, since there is a strict connection between the intrinsic properties of the rock and its σ_{ucs} (e.g. Hatzor and Palchik 1997; Přikryl 2001; 2006; Basu et al. 2009; Pappalardo and Mineo 2017), even σ_{ci} and σ_{cd} are expected to be influenced by the rock structure and texture. By analyzing these correlations in detail, data scattering resulted a bit more evident for σ_{ucs}-σ_{ci} plot (Fig. 7a), which is indeed the correlation with a slightly lower, although satisfactory, r^2 (0.91), while σ_{ucs}-σ_{cd} plot follows a less scattered trend (Fig. 7b). This is likely related to the principle of the crack initiation itself and to its strict dependence on the initial macro- and micro-structure of the rock specimen. In fact, the generation of cracks occurs when the tensile stresses induced by compression exceed the local tensile strength at the tips of the pre-existing flaws (e.g. Cai et al. 2004; Basu et al. 2013; Pappalardo et al. 2016b). Therefore, σ_{ci} is influenced by the presence of pre-existing cracks or pores and by their orientation within the rock, which can either enhance or hinder the crack initiation, leading to a more scattered relationship with σ_{ucs}. On the other hand, once the crack initiation has occurred, the rock texture does not affect the mechanical behavior of the specimen any longer. In fact, from this point, the rock is already cracked by compression and the main element driving its failure is the evolution of the cracking process. This outclasses the influence of the initial rock structure so that σ_{cd} and the final compression strength are linked by a less scattered trend (Fig. 7b).

The relationships between such considered three stress levels and the stiffness parameters indicate a mutual dependence with the elastic modulus E_{t50}, although with a poorer correlation (see r^2 in Table 4). In fact, even if it is known that a positive trend usually links σ_{ucs} and E_{t50} (e.g. D'Andrea et al. 1965; Deere and Miller 1966; Gupta and Rao 2000; Tugrul and Zarif 2000; Sabatakakis et al. 2008), such correlation is affected by a certain degree of scattering mainly due to the physical and mineralogical properties of the rock (e.g. Mineo and Pappalardo 2016a; Pappalardo et al. 2017), which can

either enhance or hinder the failure of a specimen and its deformability as above stated. Such not fully satisfactory trend suggests that E_{t50} parameter is not good enough to predict σ_{ci} and σ_{cd}, considering data available in this study. According to some literature experiences (e.g. Nassif, 2003), a similar consideration can be stated with respect to Poisson's ratio, which is not correlated with the above-mentioned parameters (Table 3).

In this perspective, summarizing the first results achieved in this section, only two reliable equations can be obtained by the statistical analysis above commented, which allow predicting crack initiation and crack damage stress quantities from σ_{ucs} (eq. 1 and 2). These equations involve all the bibliographic data, with no distinction between the rock types; therefore, in this paper we will refer to them as "general" equations, with r^2 0.91 and 0.96, respectively.

$$\sigma_{ci}(\text{MPa}) = 2.2713 + (0.4456\ \sigma_{UCS}) \qquad \textbf{eq. 1}$$

$$\sigma_{cd}(\text{MPa}) = 0.4818 + (0.8076\ \sigma_{UCS}) \qquad \textbf{eq. 2}$$

4.2 Single regression analyses for particular prediction equations

Once assessed the good correlation between analyzed data, in order to take into account a possible variability related to the different genesis of considered rocks, literature data were grouped into sedimentary (SED), metamorphic (MET) and igneous (IGN) categories. In such setting, single regression analyses, from now on referred as to "particular" relations, were carried out with the aim of retrieving equations, which could potentially be used to predict crack stress levels more precisely for each group of rocks. Outlined trends reflect the general fitting previously described, as σ_{ucs} correlates significantly with both σ_{ci} and σ_{cd} by positive linear relations. With reference to σ_{ucs} vs σ_{ci} (Fig. 8a-c), data scattering increases from SED rocks (r^2=0.97), through MET (r^2=0.92), to IGN (r^2=0.77) group. This difference could be explained by taking into account the possible differences occurring between the three rock groups. In particular, SED and MET rocks considered herein are likely to be characterized by a certain degree of primary and/or secondary porosity, although no specific information was retrieved by the analysis of literature data. In these rocks, cracks could either propagate from the tip of a pore/crack, or from the residue of a fossil, while maintaining a good correlation with σ_{ucs}. On the other hand, IGN (herein represented only by intrusive rocks) are likely to be affected by a very low porosity and by strong contacts between minerals. In this case, cracks can initiate only from peculiar weak portions of the rock, especially at grain boundaries, and their growth is strictly related to the relationship between the mineral phases and to the grain size. In fact, it is known that the grain size of rocks plays a leading role during stress, as both crack initiation stress and rock strength were found to decrease with increasing grain size (Eberhardt et al. 1999b; Nicksiar and Martin 2013, 2014). Moreover,

Brace (1972) stated that in crystalline, igneous rock, although grain boundaries are the preferred site of microcracks, intragranular cracks also occur in some of the weaker mineral constituents such as feldspar and biotite grains. This was observed also in Etna lavas by Pappalardo et al. (2017), who found that microcracks, even at mineral scale, play a key role in the rock strength, leading to a great statistical variability. Variations related to the amount and distribution of stronger and weaker minerals were also reported in literature (Tapponnier and Brace 1976; Fredrich et al. 1990; Eberhardt et al. 1999b; Nicksiar and Martin 2013). Generally, it was observed that both crack initiation and peak strength decreased as the amount of weak minerals increased.

By looking at the relation between σ_{ucs} and σ_{cd} (Fig. 8d-f) the above reported difference in scattering is reduced, because the rock is already fractured by compression when crack damage strength is reached (IGN r^2=0.89; SED r^2=0.95; MET r^2=0.97). This result confirms that once the cracking process has initiated, rock behavior is more linked to the crack propagation rather than to the initial rock structure.

Particular best-fit equations proposed for the prediction of σ_{ci} and σ_{cd} from σ_{ucs} are eq. 3 and 4 for SED, eq. 5 and 6 for MET and eq. 7 and 8 for IGN, respectively.

$$\sigma_{\mathrm{ciSED}}(\mathrm{MPa}) = (0.4866\ \sigma_{UCS}) - 0.8458 \quad \textbf{eq. 3}$$

$$\sigma_{\mathrm{cdSED}}(\mathrm{MPa}) = (0.8568\ \sigma_{UCS}) - 1.6638 \quad \textbf{eq. 4}$$

$$\sigma_{\mathrm{ciMET}}(\mathrm{MPa}) = (0.4352\ \sigma_{UCS}) + 5.2809 \quad \textbf{eq. 5}$$

$$\sigma_{\mathrm{cdMET}}(\mathrm{MPa}) = (0.8353\ \sigma_{UCS}) - 1.7635 \quad \textbf{eq. 6}$$

$$\sigma_{\mathrm{ciIGN}}(\mathrm{MPa}) = (0.4369\ \sigma_{UCS}) + 3.7609 \quad \textbf{eq. 7}$$

$$\sigma_{\mathrm{cdIGN}}(\mathrm{MPa}) = (0.7972\ \sigma_{UCS}) - 1.5905 \quad \textbf{eq. 8}$$

4.3 Multiple regression analysis for prediction models

Performed simple regression analyses demonstrated that σ_{ucs} is a good independent variable to predict crack initiation and unstable crack propagation thresholds using both general and particular equations. This is an interesting result considering that, unlike σ_{ucs}, σ_{ci} and σ_{cd} measurements are not currently routine procedures also because the main testing agencies still give no information about their accurate evaluation (Nicksiar and Martin 2012).

Based on the mutual dependence existing between σ_{ci} and σ_{cd} (Fig. 9), which are linked by a positive linear relation with a low scattering (r^2 =0.94, p=00.000), in this section results of multiple regression analyses are presented. Such approach

allowed considering more than one independent variable for the prediction of σ_{ci} and $\sigma_{cd,}$ so to achieve a more reliable prediction model (Mineo and Pappalardo 2016b).

In this perspective, two models were compiled to predict:

- σ_{ci} from σ_{ucs} and σ_{cd} (from now on referred to as prediction model 1 PM1);
- σ_{cd} from σ_{ucs} and σ_{ci} (from now on referred to as prediction model 2 PM2).

In particular, PM1 is particularly significant, because σ_{ci} evaluation in laboratory can be often a hard matter. In fact, the procedures require high-quality specimens and adequate laboratory equipment that are not always available during preliminary design stages. Furthermore, the majority of the suggested methods for identifying σ_{ci} can be time-consuming and affected by subjectivity of the user. In fact, one of the main factors influencing σ_{ci} detection is the nonlinear mechanical behaviour at low stress due to the density of pre-existing defects (Eberhardt et al. 1998; Nicksiar and Martin 2012). Such nonlinearity of the stress-strain response makes the procedures more difficult, leading to uncertainty into the determinate values.

Statistical analysis for PM1 returned a multiple r of 0.97, an adjusted r^2 of 0.94 and a *p*-value < 0.0000, while model 2 shows a multiple r of 0.99, an adjusted r^2 of 0.97 and a *p*-value < 0.0000.

Such results confirm the reliability of both σ_{ucs} and σ_{cd} as predictor values for crack initiation stress (PM1) and of both σ_{ucs} and σ_{ci} as predictor values for crack damage stress (PM2). Achieved relations are further validated by residual analyses, which show a normal distribution of residuals in both cases (Fig. 10), thus indicating that the hypothesis that residual values are only a random dataset is true. Therefore, the regression models well explain all trends in the dataset; achieved prediction equations are listed below (eqs. 9 and 10).

$$\sigma_{ci}(\mathrm{MPa}) = (0.0575\ \sigma_{UCS}) + (0.4788\sigma_{cd}) + 2.3826 \qquad \textbf{eq. 9}$$

$$\sigma_{cd}(\mathrm{MPa}) = (0.5028\ \sigma_{UCS}) + (0.690\sigma_{ci}) - 1.9919 \qquad \textbf{eq. 10}$$

5 Validation of equations

In this section, the above provided relations and their representative equations were used to test the predictability of crack initiation and damage stress levels on rock specimens properly tested, in order to establish a comparison between predicted and measured values. Such procedure, in terms of scatter plots, is one of the most common alternatives to evaluate model predictions (Pineiro et al. 2008). As already introduced, σ_{ucs}, σ_{ci} and σ_{cd} were experimentally evaluated for 132 specimens of metamorphic and sedimentary rocks (Table 2). Accordingly, σ_{ci} and σ_{cd} were predicted through equations 1-10 and results were compared with the correspondent measured ones (Fig. 11).

5.1 Prediction from single regression equations

Starting from general equations 1 and 2, predicted σ_{ci} well correlates with the corresponding measured values. Nevertheless, achieved trend shows a certain scattering, with a plot characterized by a r^2 of 0.77 (Fig. 11a). This confirms that the level of stress defining the transition between the linear elastic response and the onset of new cracks still maintains a certain degree of uncertainty, mainly due to the intrinsic features of tested rocks (e.g. presence of pre-existing flaws, porosity), playing a leading role in the crack initiation process itself. This is consistent with the observations of Hidalgo and Nordlund (2013), who stated that further studies are needed to more clearly understand how intrinsic rock features are related to cracking processes. On the other hand, a better fit is achieved for σ_{cd}, with a r^2 of 0.87 and a *p*-value < 0.0000 (Fig. 11b), reflecting the general trend already shown in Figure 7 and testifying the goodness of the prediction model, keeping in consideration that natural materials as rocks do not follow strict mathematical laws. In this case, the most scattered data are related to specimens of meta-granodiorite and meta-leucogranite, probably due to peculiar features of such laboratory samples, although the fitting is however satisfactory

Passing through equations 3 to 6 (particular equations) to predict crack stress thresholds (Fig. 11c-d), no relevant differences are observed with respect to the previous predicted vs measured plots. In fact, achieved graphs can be almost overlapped and r^2 values related to such plots are almost the same. This means that no appreciable differences can be outlined between general and particular equations, proving the suitability of the proposed relations for SED and MET.

5.2 Prediction from multiple regression equations

By operating a similar comparison between predicted and measured values through PM1 and PM2 (two independent variables), a more precise estimation of the datum is achieved (Fig. 12). In fact, compared to the previous plots, a more satisfactory trend is achieved herein, thus proving the good intuition of predicting σ_{ci} and σ_{cd} from more than one independent variable. In particular, σ_{ci} plot (Fig. 12a) is characterized by a higher coefficient of correlation than those

shown by both the general and the particular equations (r^2=0.82). In fact, the diagram (Fig. 12a) shows a less scattered plot, although the influence of the intrinsic properties of the rock cannot be excluded. Similarly, PM2 allows achieving a correlation coefficient close to 1 (Fig. 12b) and a determination coefficient of 0.90 against 0.87 of particular and general equations, proving that the estimation of crack damage stress is more precise if the crack initiation stress value is known along with σ_{ucs}. It should be underlined that provided equations can be employed only if σ_{ci} and σ_{cd} are, in turn, known besides of σ_{ucs}.

6 Conclusions

In this work, empirical equations for the prediction of the crack initiation and damage thresholds (i.e. σ_{ci} and σ_{cd}) for intact rocks were developed by analysing a dataset consisting of the main mechanical parameters of more than 480 rock specimens collected from literature. Unconfined compression test results of igneous, metamorphic and sedimentary rock types were statistically treated by single and multiple regression approaches to study the mutual dependence between the main mechanical parameters, with particular reference to crack initiation (σ_{ci}) and crack damage (σ_{cd}) stresses. Such analyses allowed providing "general" prediction equations, taking into account the entire dataset, and "particular" prediction equations, specific for each group of rocks (i.e. igneous, metamorphic and sedimentary). Results were validated by the empirical estimation of σ_{ci} and σ_{cd} on 132 rock specimens, properly tested in laboratory to obtain reference values. Measured and calculated data were compared and the results confirm that σ_{ci} and σ_{cd} are well correlated with σ_{ucs} regardless of the wide spectrum of petrographic, mineralogical and textural features, also according to previous findings. In particular, proposed trends proved that crack initiation stress level is likely to be influenced by the rock texture, which can either enhance or hinder the crack initiation process, leading to a more scattered relationship with σ_{ucs}. Conversely, once crack initiation has occurred and the compression proceeds, the rock texture seems not to affect the mechanical behavior of the specimen any longer. In fact, from this point, the mechanical attitude of the rock, already damaged by compression, is mainly driven by the evolution of the cracking process. This outclasses the influence of the initial rock structure so that σ_{cd} and the peak strength are linked by a less scattered trend. In this way, Uniaxial Compressive Strength proved a good variable to predict crack initiation and damage stress levels, due to the satisfactory trends linking such parameters. On the contrary, no suitable relationships were found between crack stress thresholds and stiffness properties (i.e. Young's modulus and Poisson's ratio).

General and particular prediction equations proved a good tool for the empirical estimation of σ_{ci} and σ_{cd}, thus representing a valid alternative to the laboratory procedures. Moreover, a greater prediction accuracy is achieved by using the

Prediction Models resulting from the multiple regression analyses, which take into account two known variables. This aspect gains a peculiar importance, especially when time-consuming experimental procedures need to be avoided.

The comparisons between predicted and actual experimental data allow validating the goodness of the proposed empirical equations and lay the foundations for future studies, possibly aimed at developing prediction models involving also mineralogical, textural and physical properties. Nevertheless, such equations are practical and accurate enough for preliminary engineering design dealing with stress-induced brittle fracturing prior to performing laboratory tests. Eventually, the obtained equations can be particularly useful for predicting σ_{ci} since most of the methods proposed for its evaluation can suffer from uncertainty and subjectivity.

Acknowledgements

The Authors are grateful to the Servizi Geotecnici Liguri S.r.l. Soil and rock mechanics laboratory (Vado Ligure, Italy) for providing laboratory equipment. The Authors wish to thank also the Editor-in-Chief Martin Gordon Culshaw and the two anonymous referees for their helpful comments and suggestions that improved this paper.

References

Amann F, Button EA, Evans KF, Gischig VS, Blümel M (2011) Experimental study of the brittle behavior of clay shale in rapid unconfined compression. Rock Mech Rock Eng 44(4):415-430. doi:10.1007/s00603-011-0156-3

Andersson C, Martin CD (2009) The Äspö pillar stability experiment: part II-rock mass response to coupled excavation induced and thermal-induced stresses. Int J Rock Mech Min Sci 46(5):865-878. doi:10.1016/j.ijrmms.2009.03.002

ASTM (2001) American Society for Testing and Materials. ASTM Standards on Disc, 04.08. West Conshohocken, PA

Basu A, Celestino TB, Bortolucci AA (2009) Evaluation of rock mechanical behaviours under uniaxial compression for different weathering grades. Rock Mech Rock Eng 42:73–93. doi:10.1007/s00603-008-0170-2

Basu A, Mishra DA, Roychowdhury K (2013) Rock failure modes under uniaxial compression, Brazilian, and point load tests. Bull Eng Geol Env 72(3-4):457-475. doi:10.1007/s10064-013-0505-4

Bedi A, Harrison JP (2013) Characterisation and propagation of epistemic uncertainty in rock engineering: A slope stability example. In Proceedings of ISRM international symposium Eurock, pp. 105-110

Bieniawski ZT (1967) Mechanism of brittle fracture of rock, part II—experimental studies. Int J Rock Mech Min Sci Geomech Abstr 4(4):407–423

Brace WF, Paulding B, Scholz C (1966) Dilatancy in the fracture of crystalline rocks. J Geophys Res 71:3939-3953

Brace WF, Silver E, Hadley K, Goetze C (1972) Cracks and pores: A closer look. Science 178(4057):162-164.

Cai M, Kaiser PK, Tasaka Y, Maejima T, Morioka H, Minami M (2004) Generalized crack initiation and crack damage stress thresholds of brittle rock masses near underground excavations. Int J Rock Mech Min Sci 41(5):833-847. doi:10.1016/j.ijrmms.2004.02.001

Cai M (2010) Practical estimates of tensile strength and Hoek–Brown strength parameter mi of brittle rocks. Rock Mech Rock Eng 43(2):167-184. doi:10.1007/s00603-009-0053-1

Cai M, Kaiser PK (2014) In-situ rock spalling strength near excavation boundaries. Rock Mech Rock Eng 47:659-675. doi:10.1007/s00603-013-0437-0

Chang SH, Lee CI (2004) Estimation of cracking and damage mechanisms in rock under triaxial compression by moment tensor analysis of acoustic emission. Int J Rock Mech Min Sci 41(7):1069-1086. doi:10.1016/j.ijrmms.2004.04.006

Contrafatto L, Cuomo M, Gazzo S (2016) A concrete homogenisation technique at meso-scale level accounting for damaging behaviour of cement paste and aggregates. Computers and Structures, 173, 1-18.

Damjanac B, Fairhurst C (2010) Evidence for a long-term strength threshold in crystalline rock. Rock Mech Rock Eng 43(5):513-531. doi:10.1007/s00603-010-0090-9

D'Andrea DV, Fischer RL, Fogelson DE (1965) Prediction of compressive strength of rock from other properties. US Bureau of Mines Report, Investigation no 6702

Deere DU, Miller RP (1966) Engineering classification and index properties for intact rock. Technical report n. AFWL-TR-65-116, Air Force Weapons Laboratory, New Mexico

Diederichs MS, Kaiser PK, Eberhardt E (2004) Damage initiation and propagation in hard rock during tunnelling and the influence of near-face stress rotation. Int J Rock Mech Min Sci 41(5):785-812. doi:10.1016/j.ijrmms.2004.02.003

Diederichs MS (2007) The 2003 Canadian Geotechnical Colloquium: mechanistic interpretation and practical application of damage and spalling prediction criteria for deep tunnelling. Can Geotech J 44:1082-1116. doi:10.1139/T07-033

Eberhardt E, Stead D, Stimpson B, Read RS (1998) Identifying crack initiation and propagation thresholds in brittle rock. Can Geotech J 35(2):222-233. doi:10.1139/t97-091

Eberhardt E, Stead D, Stimpson B (1999a) Quantifying progressive pre-peak brittle fracture damage in rock during uniaxial compression. Int J Rock Mech Min Sci 36(3):361-380. doi:10.1016/S0148-9062(99)00019-4

Eberhardt E, Stimpson B, Stead D (1999b) Effect of grain size on the initiation and propagation threshold of stress-induced brittle fracture. Rock Mech Rock Eng 32(2):81-99. doi:10.1007/s006030050026

Eloranta P, Hakala P (1998) Laboratory testing of Kivetty porphyritic granodiorite in borehole KI-KR10. Posiva 98-49, Finland

Eloranta P, Hakala P (1999a) Laboratory testing of Hästholmen pyterlite in borehole HH-KR6. Posiva 98-26, Finland

Eloranta P, Hakala P (1999b) Laboratory testing of Hästholmen equigranular rapakivi granite in borehole HH-KR6. Posiva 98-47, Finland

Fredrich JT, Evans B, Wong TF (1990) Effect of grain size on brittle and semibrittle strength: Implications for micromechanical modelling of failure in compression. J Geophys Res 95(B7):10907-10920.

Fonseka GM, Murrell SAF, Barnes P (1985) Scanning electron microscope and acoustic emission studies of crack development in rocks. Int J Rock Mech Min Sci Geomech Abstr 22(5):273-289.

Gatelier N, Pellet F, Loret B (2002) Mechanical damage of an anisotropic porous rock in cyclic triaxial tests. Int J Rock Mech Min Sci 39(3):335-354. doi:10.1016/S1365-1609(02)00029-1

Gupta AS, Rao KS (2000) Weathering effects on the strength and deformational behaviour of crystalline rocks under uniaxial compression state. Eng Geol 56(3):257-274. doi:10.1016/S0013-7952(99)00090-3

Hajiabdolmajid V, Kaiser P (2003) Brittleness of rock and stability assessment in hard rock tunneling. Tunn Undergr Sp Tech 18(1):35-48. doi:10.1016/S0886-7798(02)00100-1

Hatzor YH, Palchik V (1997) The influence of grain size and porosity on crack initiation stress and critical flaw length in dolomites. Int J Rock Mech Min Sci 34(5):805-816. doi:10.1016/S1365-1609(96)00066-6

Heikkilä E, Hakala M (1998a) Laboratory testing of Romuvaara tonalite gneiss in borehole RO-KR10. POSIVA-98-06e, Finland

Heikkilä E, Hakala M (1998b) Laboratory testing of Kivetty granite in borehole KI-KR10. POSIVA-98-21e, Finland

Hidalgo KP, Nordlund E (2013) Comparison between stress and strain quantities of the failure-deformation process of fennoscandian hard rocks using geological information. Rock Mech Rock Eng 46(1):41-51. doi:10.1007/s00603-012-0242-1

Hoek E, Bieniawski ZT (1965) Brittle fracture propagation in rock under compression. Int J Fracture Mech 1(3):137-155

Hoek E, Kaiser PK, Bawden WF (1995) Support of Underground Excavations in Hard Rock. A.A. Balkema, Rotterdam, 215 p.

Hoek E, Brown ET (1997) Practical estimates of rock mass strength. Int J Rock Mech Min Sci Geomech Abstr 34(8):1165-1186. doi:10.1016/S1365-1609(97)80069-X

Huang J, Wang Z, Zhao Y (1993) The development of rock fracture from microfracturing to main fracture formation. Int J Rock Mech Min Sci Geomech Abstr 30(7):925-928. doi:10.1016/0148-9062(93)90046-G

Klein E, Reuschlé T (2004) A pore crack model for the mechanical behaviour of porous granular rocks in the brittle deformation regime. Int J Rock Mech Min Sci 41(6):975-986. doi:10.1016/j.ijrmms.2004.03.003

Lajtai EZ (1974) Brittle fracture in compression. Int J Fract Mech 10:525-536.

Lajtai EZ (1998) Microscopic fracture processes in a granite. Rock Mech Rock Eng 31(4):237-250. doi:10.1007/s006030050023

Liang WG, Zhao YS, Xu SG, Dusseault MB (2011) Effect of strain rate on the mechanical properties of salt rock. Int J Rock Mech Min Sci 48(1):161-167. doi:10.1016/j.ijrmms.2010.06.012

Lin QX, Liu YM, Tham LG, Tang CA, Lee PKK, Wang J (2009) Time-dependent strength degradation of granite. Int J Rock Mech Min Sci 46(7):1103-1114. doi:10.1016/j.ijrmms.2009.07.005

Martin CD (1993) The strength of massive Lac du Bonnet granite around underground openings. Doctoral thesis, University of Manitoba, Winnipeg, Man.

Martin CD, Chandler NA (1994) The progressive fracture of Lac du Bonnet granite. Int J Rock Mech Min Sci Geomech Abstr 31(6): 643-659. doi:10.1016/0148-9062(94)90005-1

Martin CD (1997) Seventeenth Canadian geotechnical colloquium: the effect of cohesion loss and stress path on brittle rock strength. Can Geotech J 34(5): 698-725. doi: 10.1139/t97-030

Martin CD, Kaiser PK, McCreath DR (1999) Hoek-Brown parameters for predicting the depth of brittle failure around tunnels. Can Geotech J 36(1): 136-151. doi:10.1139/t98-072

Martin CD, Christiansson R (2009) Estimating the potential for spalling around a deep nuclear waste repository in crystalline rock. Int J Rock Mech Min Sci 46: 219-228. doi:10.1016/j.ijrmms.2008.03.001

Mineo S, Pappalardo G, D'Urso A, Calcaterra D (2017) Event tree analysis for rockfall risk assessment along a strategic mountainous transportation route. Environ Earth Sci, 76:620. DOI 10.1007/s12665-017-6958-1

Mineo S, Pappalardo G (2016a) Preliminary results on the estimation of porosity in intact rock through InfraRed Thermography. Rend. Online Soc. Geol. It., Vol. 41, 317-320. doi: 10.3301/ROL.2016.157

Mineo S, Pappalardo G (2016b) The Use of Infrared Thermography for Porosity Assessment of Intact Rock. Rock Mech Rock Eng 49 (8):3027-3039. doi: 10.1007/s00603-016-0992-2

Nassif A (2003) Stress-strain relationship for weak rocks. In Di Benedetto et al. Deformation characteristics of Geomaterials/Comportement Des Sols Et Des Roches Tendres, 415-419.

Nicksiar M, Martin CD (2012) Evaluation of Methods for Determining Crack Initiation in Compression Tests on Low-Porosity Rocks. Rock Mech Rock Eng 45(4): 607-617. doi:10.1007/s00603-012-0221-6

Nicksiar M (2013) Effective parameters on crack initiation stress in low porosity rocks. Doctoral thesis, University of Alberta, Canada.

Nicksiar M, Martin CD (2013) Crack initiation stress in low porosity crystalline and sedimentary rocks. Eng Geol 154: 64-76. doi:10.1016/j.enggeo.2012.12.007

Nicksiar M, Martin CD (2014) Factors affecting crack initiation in low porosity crystalline rocks. Rock Mech Rock Eng 47(4):1165-1181. doi:10.1007/s00603-013-0451-2

Palchik V, Hatzor YH (2002) Crack damage stress as a composite function of porosity and elastic matrix stiffness in dolomites and limestones. Eng Geol 63(3):233-245. doi:10.1016/S0013-7952(01)00084-9

Pappalardo G (2015). Correlation between P-wave velocity and physical-mechanical properties of intensely jointed dolostones, Peloritani Mounts, NE Sicily. Rock Mech Rock Eng 48:1711-1721. doi:10.1007/s00603-014-0607-8.

Pappalardo G, Mineo S (2016) Microstructural controls on physical and mechanical properties of dolomite rocks. Rend Online Soc Geol It 41:321-324. doi: 10.3301/ROL.2016.158

Pappalardo G, Mineo S (2017) Investigation on the mechanical attitude of basaltic rocks from Mount Etna through InfraRed Thermography and laboratory tests. Constr Build Mater 134, 228–235. doi: 10.1016/j.conbuildmat.2016.12.146

Pappalardo G, Mineo S, Marchese G (2013) Effects of cubical specimen sizing on uniaxial compressive strength of Etna volcanic rocks (Italy). Ital J Eng Geol Env 2:5-14. doi: 10.4408/IJEGE.2013-02.O-03

Pappalardo G, Punturo R, Mineo S, Ortolano G, Castelli F (2016a) Engineering Geological and Petrographic Characterization of Migmatites Belonging to the Calabria-Peloritani Orogen (Southern Italy). Rock Mech Rock Eng 49:1143-1160. doi: 10.1007/s00603-015-0808-9

Pappalardo G, Mineo S, Monaco C (2016b) Geotechnical characterization of limestones employed for the reconstruction of a UNESCO world heritage Baroque monument in southeastern Sicily (Italy). Eng Geol 212:86-97. doi: 10.1016/j.enggeo.2016.08.004

Pappalardo G, Punturo R, Mineo S, Contrafatto L (2017) The role of porosity on the engineering geological properties of 1669 lavas from Mount Etna. Eng Geol 221:16-28. doi:10.1016/j.enggeo.2017.02.020

Pelli F, Kaiser PK, Morgenstern NR (1991) An interpretation of ground movements recorded during construction of the Donkin-Morien tunnel. Can Geotech J 28(2): 239-254.

Pepe G, Piazza M, Cevasco A (2015) Geomechanical characterization of a highly heterogeneous flysch rock mass by means of the GSI method. Bull Eng Geol Env 74:465-477. doi:10.1007/s10064-014-0642-4

Pepe G, Cevasco A, Berardi R (2016) Crack initiation and damage thresholds in some brittle metamorphic rock types. Rend Online Soc Geol It 41:325-328. doi: 10.3301/ROL.2016.159

Pepe G, Cevasco A, Gaggero L, Berardi R (2017) Variability of intact rock mechanical properties for some metamorphic rock types and its implications on the number of test specimens. Bull Eng Geol Environ 76:629-644. doi: 10.1007/s10064-016-0912-4

Perras MA, Diederichs MS (2014) A review of the tensile strength of rock: concepts and testing. Geotech Geol Eng 32(2): 525-546. doi:10.1007/s10706-014-9732-0

Phoon KK, Kulhawy FH (1999) Evaluation of geotechnical property variability. Can Geotech J 36(4):625-639. doi:10.1139/t99-039

Pineiro G, Perelman S, Guershman JP, Paruelo JM (2008) How to evaluate models: Observed vs. predicted or predicted vs. observed? Ecological Modelling 216:316-322. doi:10.1016/j.ecolmodel.2008.05.006

Prakoso WA, Kulhawy FH (2011) Effects of testing conditions on intact rock strength and variability. Geotech Geol Eng 29(1):101-111. doi:10.1007/s10706-010-9356-y

Přikryl R (2001) Some microstructural aspects of strength variation in rocks. Int J Rock Mech Min Sci Geomech. Abstr 38(5):671-682. doi:10.1016/S1365-1609(01)00031-4

Přikryl R (2006) Assessment of rock geomechanical quality by quantitative rock fabric coefficients: limitations and possible source of misinterpretations. Eng Geol 87:149-162. doi: 10.1016/j.enggeo.2006.05.011

Ranjith PG, Jasinge D, Choi SK, Mehic M, Shannon B (2010) The effect of CO2 saturation on mechanical properties of Australian black coal using acoustic emission. Fuel 89(8):2110-2117. doi:10.1016/j.fuel.2010.03.025

Read RS, Chandler NA, Dzik EJ (1998) In situ strength criteria for tunnel design in highly-stressed rock masses. Int J Rock Mech Min Sci 35(3):261-278. doi:10.1016/S0148-9062(97)00302-1

Read RS (2004) 20 years of excavation response studies at AECL's Underground Research Laboratory. Int J Rock Mech Min Sci 41(8):1251-1275. doi:10.1016/j.ijrmms.2004.09.012

Rojat F, Labiouse V, Kaiser PK, Descoeudres F (2009) Brittle rock failure in Steg Lateral Adit of the Lötschberg Base Tunnel. Rock Mech Rock Eng 42:341-359. doi: 10.1007/s00603-008-0015-z

Sabatakakis N, Koukis G, Tsiambaos G, Papanakli S (2008) Index properties and strength variation controlled by microstructure for sedimentary rocks. Eng Geol 97(1):80-90. doi:10.1016/j.enggeo.2007.12.004

Sari M, Karpuz C (2006) Rock variability and establishing confining pressure levels for triaxial tests on rocks. Int J Rock Mech Min Sci 43:328-335. doi: 10.1016/j.ijrmms.2005.06.010

Stacey TR (1981) A simple extension strain criterion for fracture of brittle rock. Int J Rock Mech Min Sci Geomech Abstr 18: 469-474.

Takarli M, Prince W, Siddique R (2008) Damage in granite under heating/cooling cycles and water freeze–thaw condition. Int J Rock Mech Min Sci 45(7):1164-1175. doi:10.1016/j.ijrmms.2008.01.002

Tapponnier P, Brace WF (1976) Development of stress-induced microcracks in Westerly granite. Int J Rock Mech Min. Sci Geomech Abstr 13(4):103-112

Terzaghi K (1946) Rock defects and loads in tunnel supports. Rock tunneling with steel supports. R.V. Proctor and T.L. White, eds., The Commercial Shearing and Stamping Co., Youngstown, Ohio, 17-99.

Thuro K, Plinninger RJ, Zäh S, Schütz S (2001) Scale effects in rock strength properties. Part 1: Unconfined compressive test and Brazilian test. In: Rock Mechanics-A Challenge for Society. Swets & Zeitlinger Lisse, pp 169-174

Tugrul A, Zarif IH (2000) Engineering aspects of limestone weathering in Istanbul, Turkey. Bull Eng Geol Env 58(3):191-206. doi:10.1007/s100640050075

Wawersik WR, Fairhurst C (1970) A study of brittle rock fracture in laboratory compression experiments. Int J Rock Mech Min Sci Geomech Abstr 7(5):561-575

Xue L, Qin L, Sun Q, Wang Y, Lee LM, Li W (2014) A study on crack damage stress thresholds of different rock types based on uniaxial compression tests. Rock Mech Rock Eng 47(4):1183-1195. doi:10.1007/s00603-013-0479-3

Table Captions

Table 1 Summary of the available intact rock data found in the literature including the number of specimens

Table 2 Summary of the tested specimens for each rock type and main mineralogical features (data from Pepe et al. 2015, 2016, 2017).

Table 3 Summary of the main statistical information on the experimental results (CV coefficient of variation)

Table 4 Equations and r^2 of the statistical correlations with E_{t50} and ν_{t50}.

Figure captions

Figure 1 Typical stress-strain curves of brittle intact rock specimen recorded under uniaxial compression together with the stages of crack development.

Figure 2 Suggested methods for determining crack initiation: a, b) volumetric strain methods; c, d, e) lateral strain methods; f) acoustic emission methods (modified after Nicksiar and Martin 2012)

Figure 3 Lateral Strain Response (LSR) method: a) determination of the crack damage stress σ_{cd}; b) determination of the linear lateral reference line and of the change in lateral strain (ΔLSR); c) determination of the crack initiation stress σ_{ci} (modified after Pepe et al. 2016).

Figure 4 Statistical variability among stress levels retrieved from literature data, with specific reference to sedimentary (SED), metamorphic (MET) and igneous (IGN) rocks.

Figure 5 Rock core test specimen preparation (a, b); representative tested specimens for different rock types (MLC meta-leucogranite, MGT meta-granite, MSG meta-syenogranite; MMZ meta-monzonite; MGD meta-granodiorite, LIM limestone); example of specimens before and after test (d, e).

Figure 6 Statistical variability among experimental data.

Figure 7 Scatterplots and correlation functions between a) σ_{ci} and σ_{ucs}; b) σ_{cd} and σ_{ucs}, with prediction and confidence regression bands at 0.95 confidence level.

Figure 8 Scatterplots and correlation functions between σ_{ci} and σ_{ucs} for a) SED; b) MET; c) IGN, and between σ_{cd} and σ_{ucs} for d) SED; e) MET; f) IGN, with prediction and confidence regression bands at 0.95 confidence level.

Figure 9 Correlation matrix between σ_{ci} and σ_{cd}. Prediction and confidence regression bands in the scatterplot are at 0.95 confidence level.

Figure 10 Distribution of residuals for Model 1 (a) and Model 2 (b).

Figure 11 Predicted vs measured values of σ_{ci} and σ_{cd} by general equations 1 (a) and 2 (b), respectively, and by particular equations 3 and 5 (c), 4 and 6 (d).

Figure 12 Predicted vs measured values of σ_{ci} and σ_{cd} by PM1 (a) and PM2 (b).

Figure1

Click here to download Figure Figure-1.tif

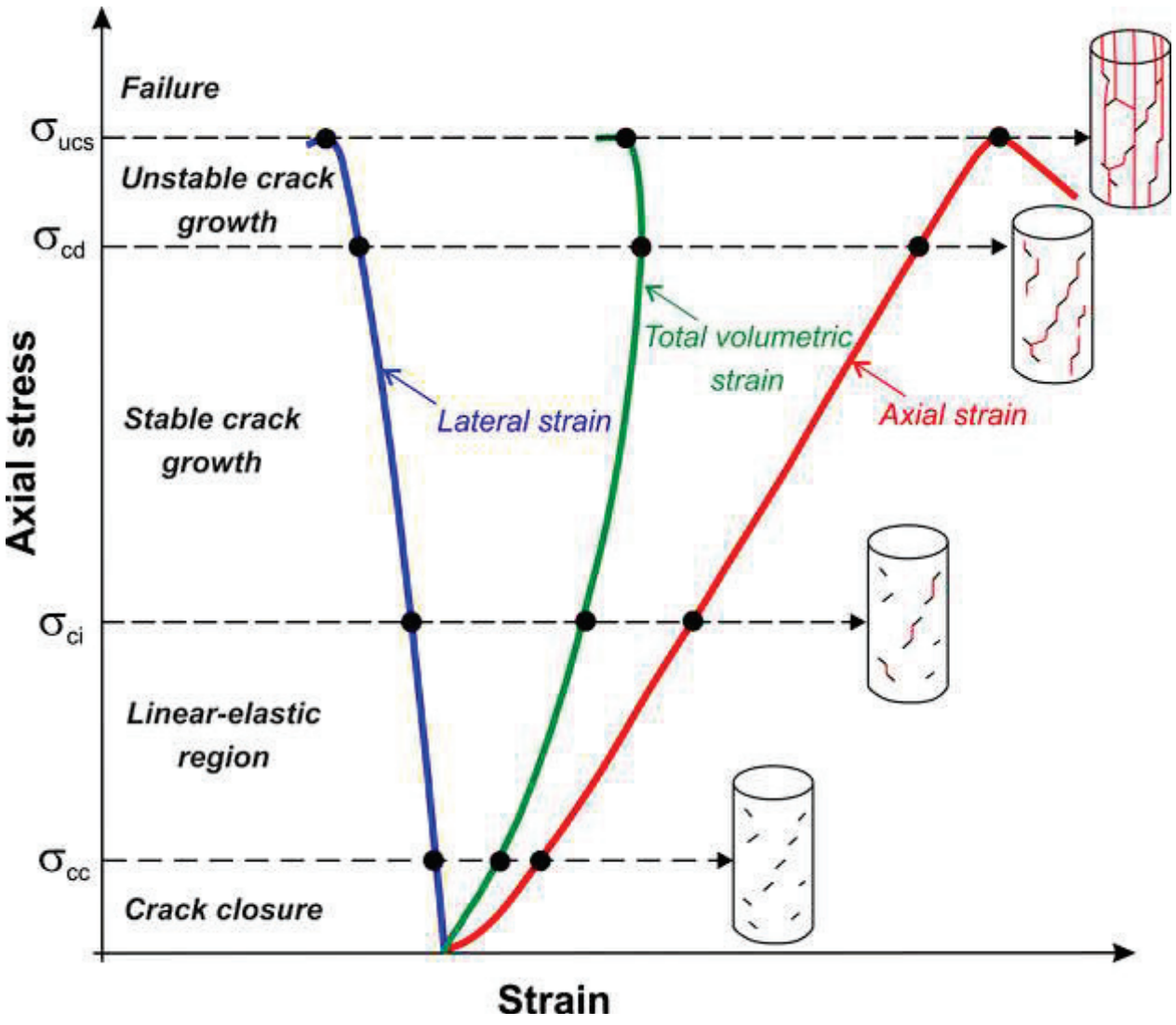

Figure2

Click here to download Figure Figure-2.tif

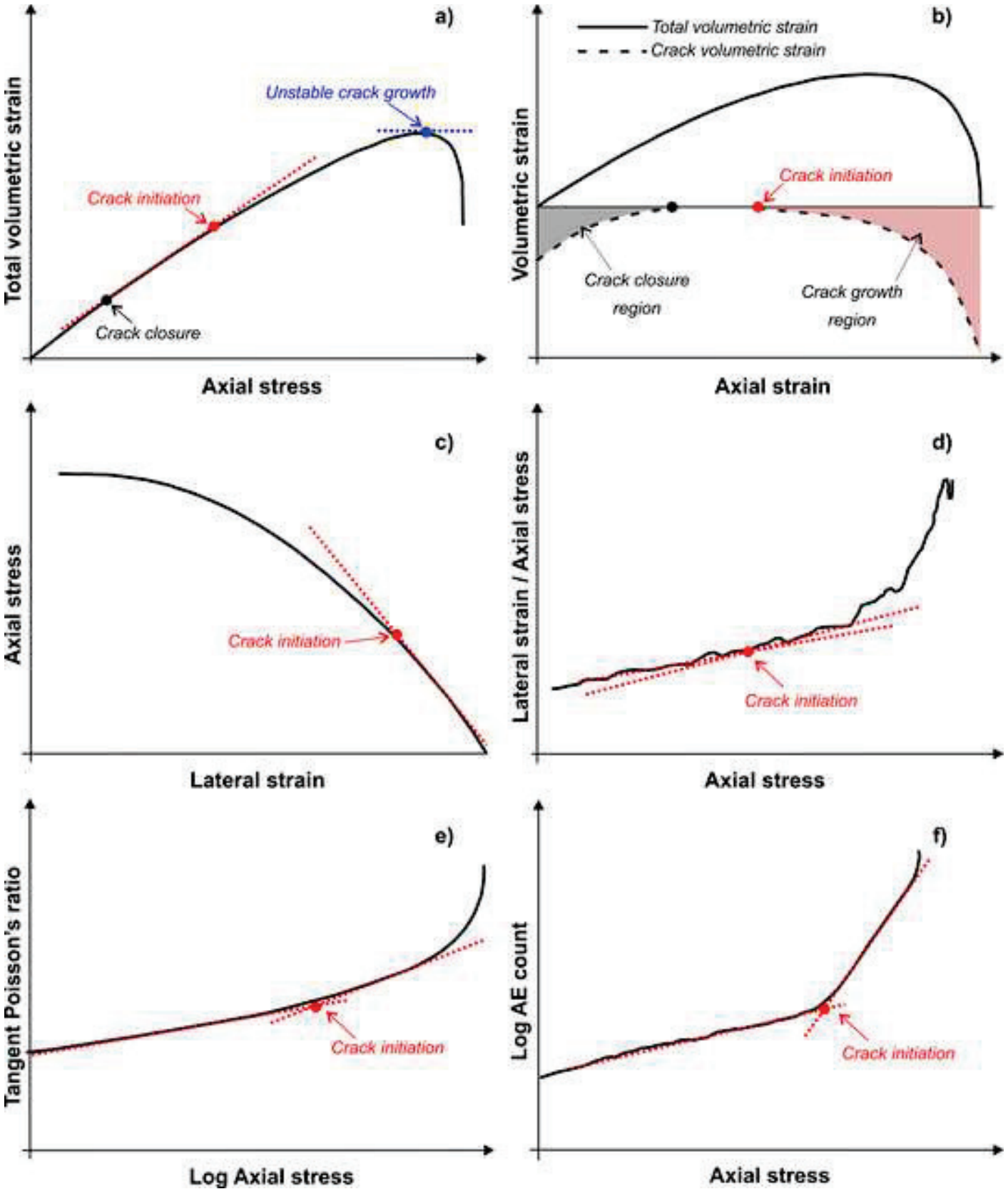

Figure3

Click here to download Figure Figure-3.tif

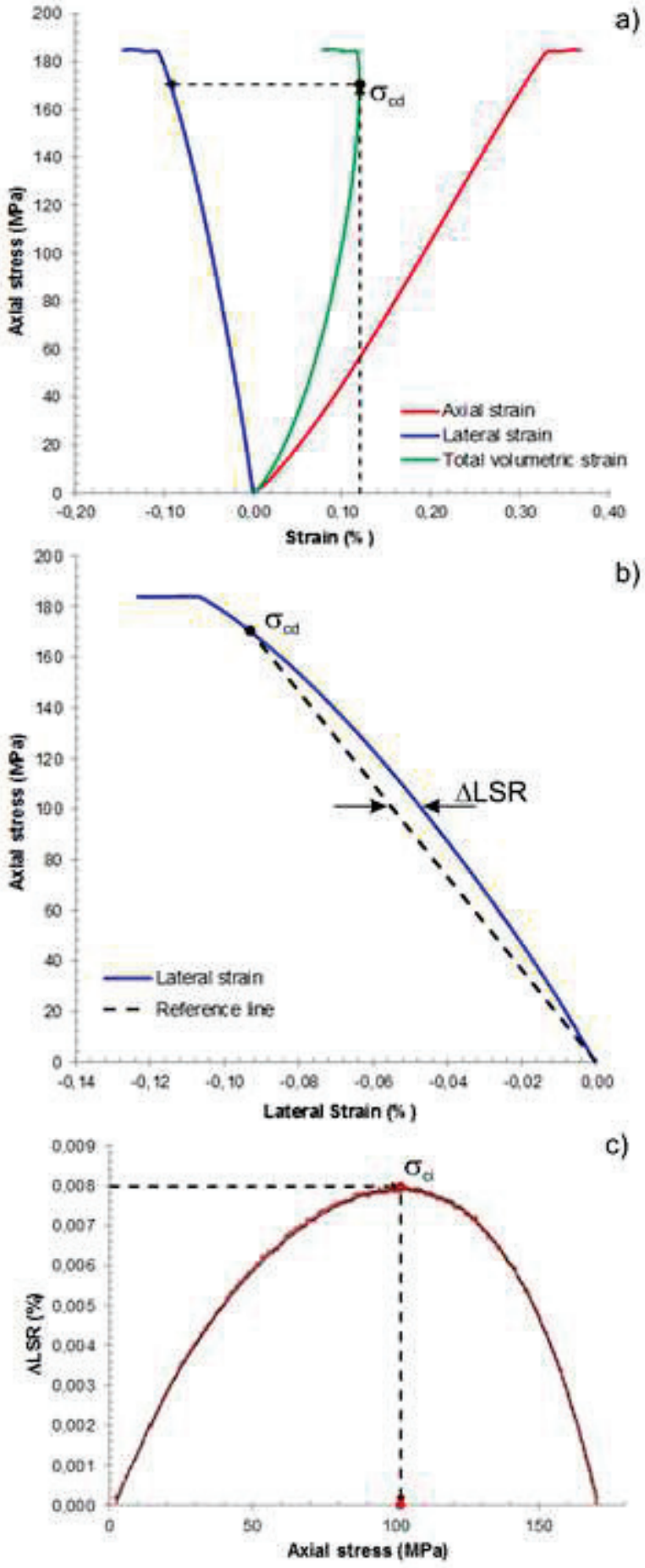

Figure4

Click here to download Figure Fig. 4.tif

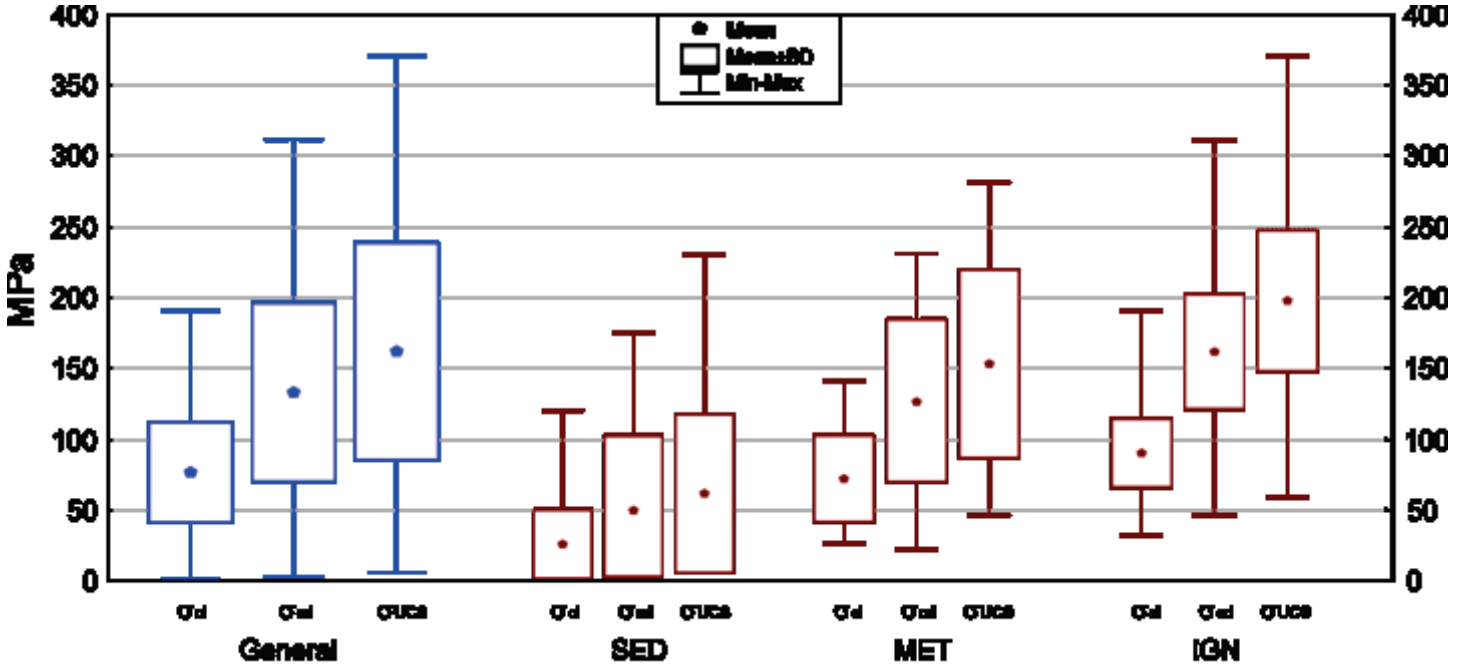

Figure5

Click here to download Figure Figure-5.tif

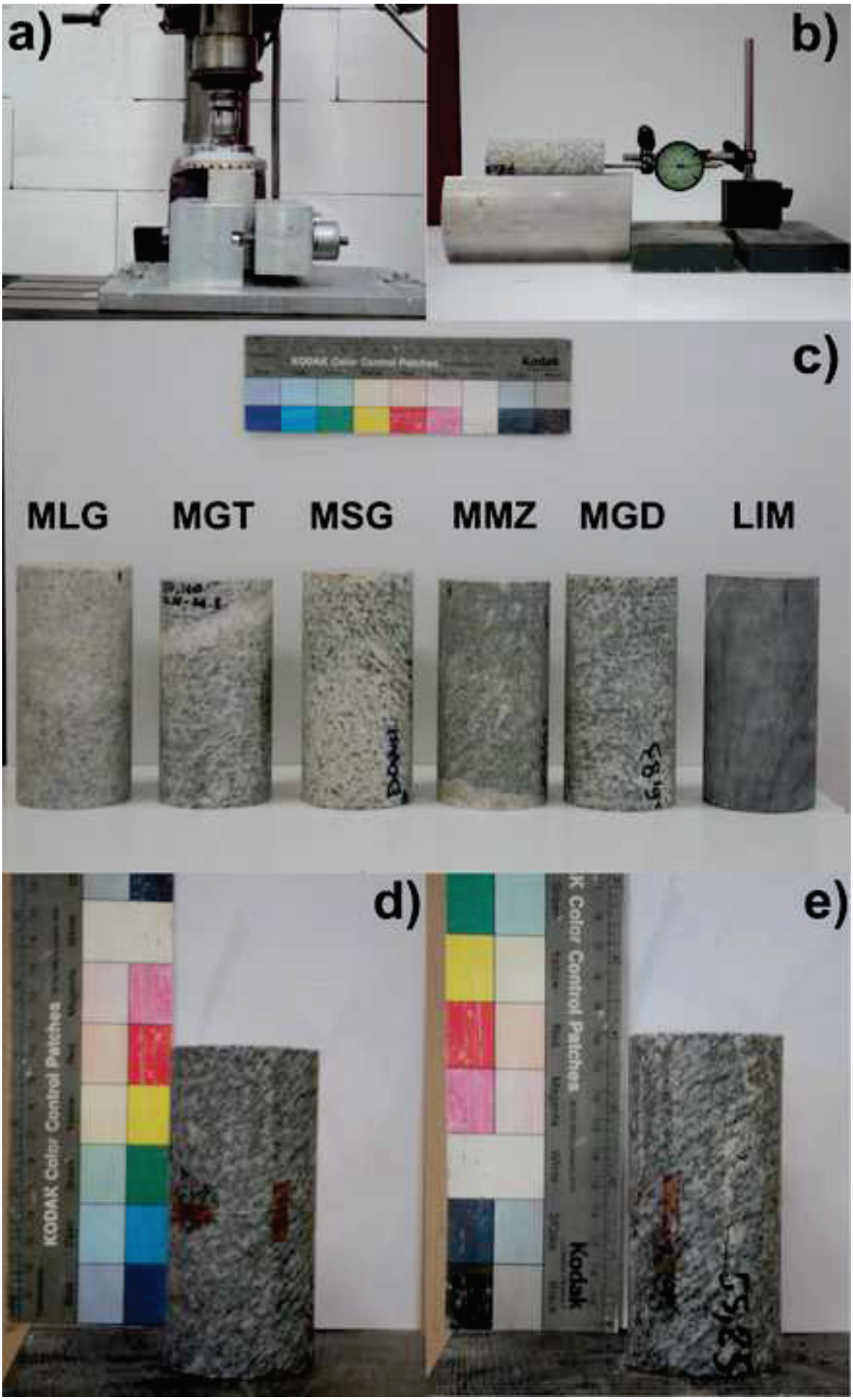

Figure6

Click here to download Figure Fig 6..tif

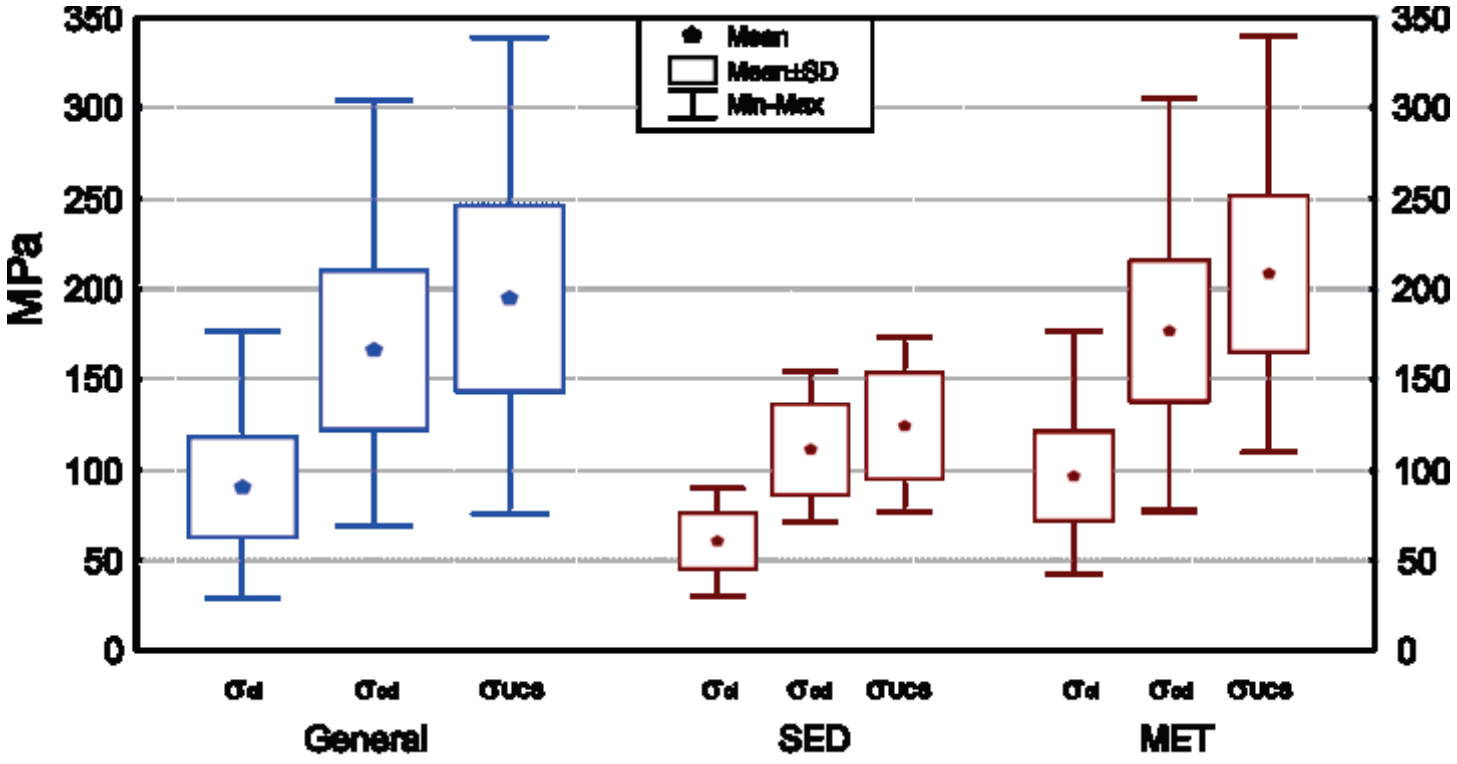

Figure7

Click here to download Figure Fig 7..tif

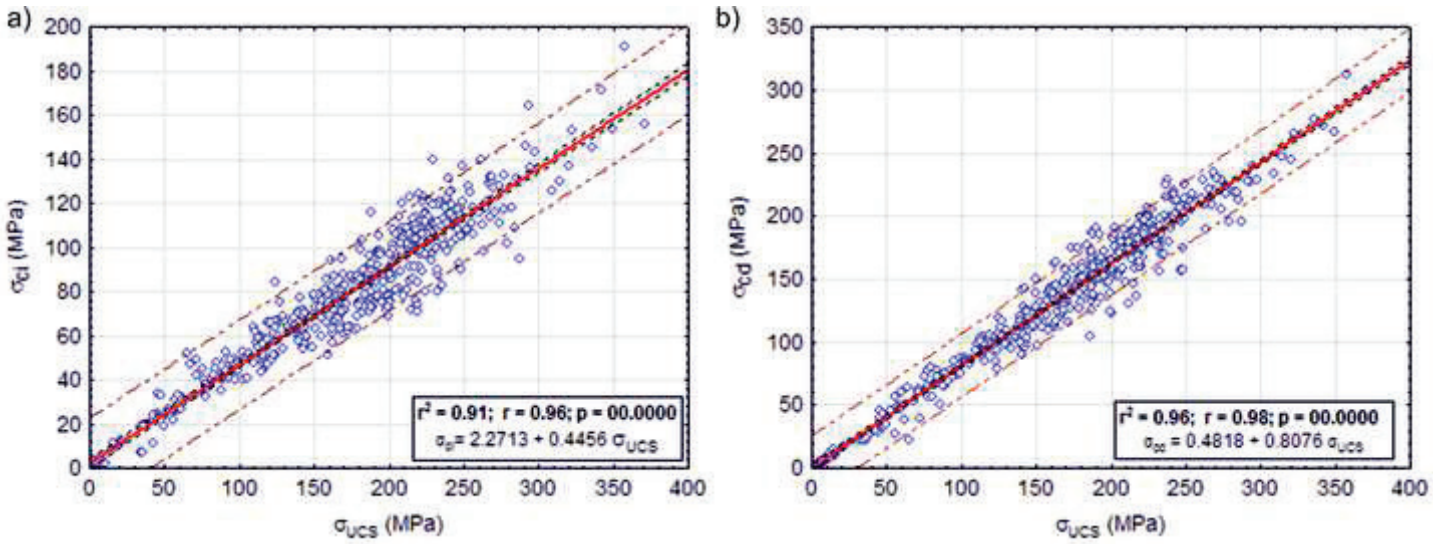

Figure8

Click here to download Figure Fig 8..tif

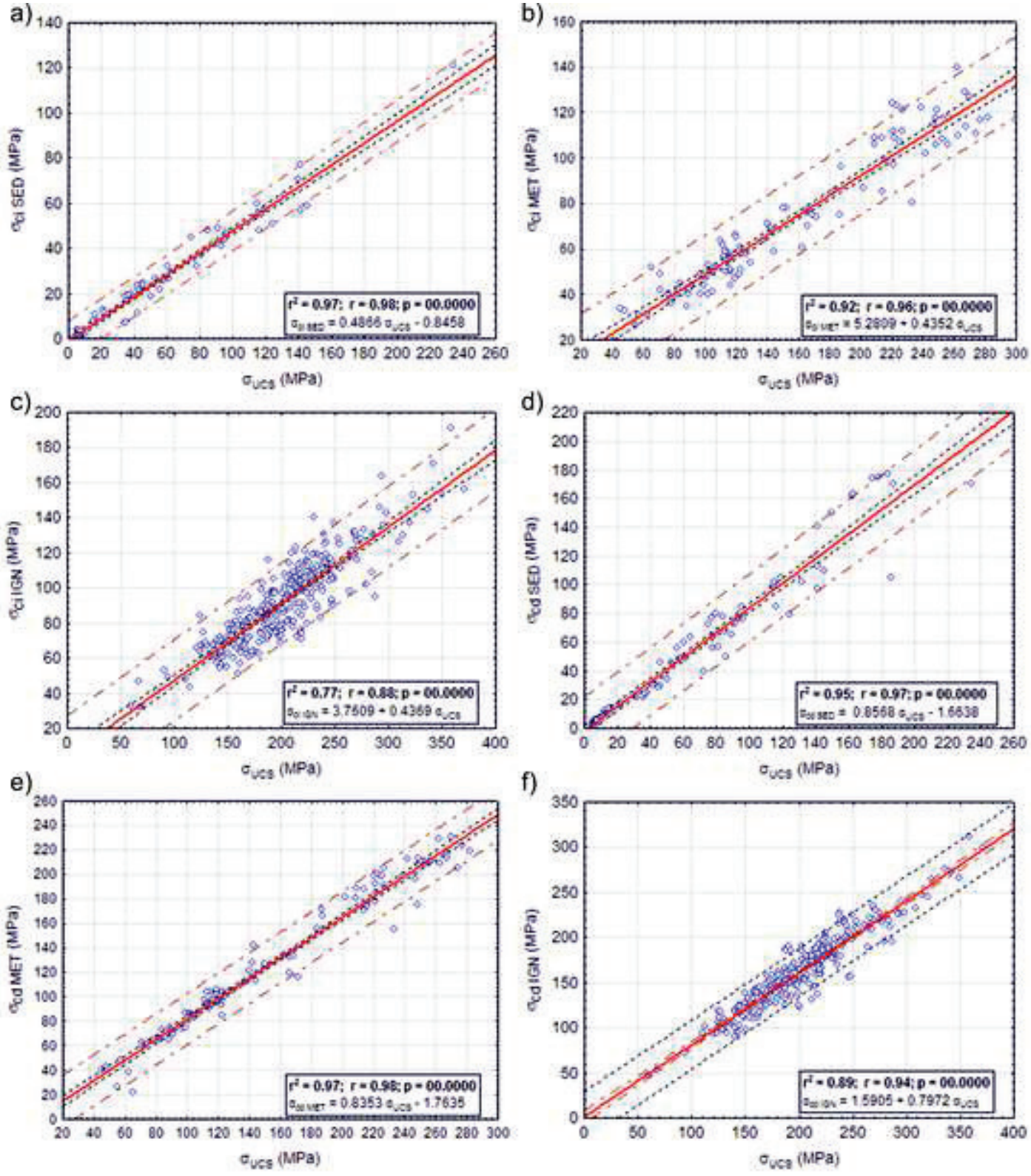

Figure9

Click here to download Figure Fig 9..tif

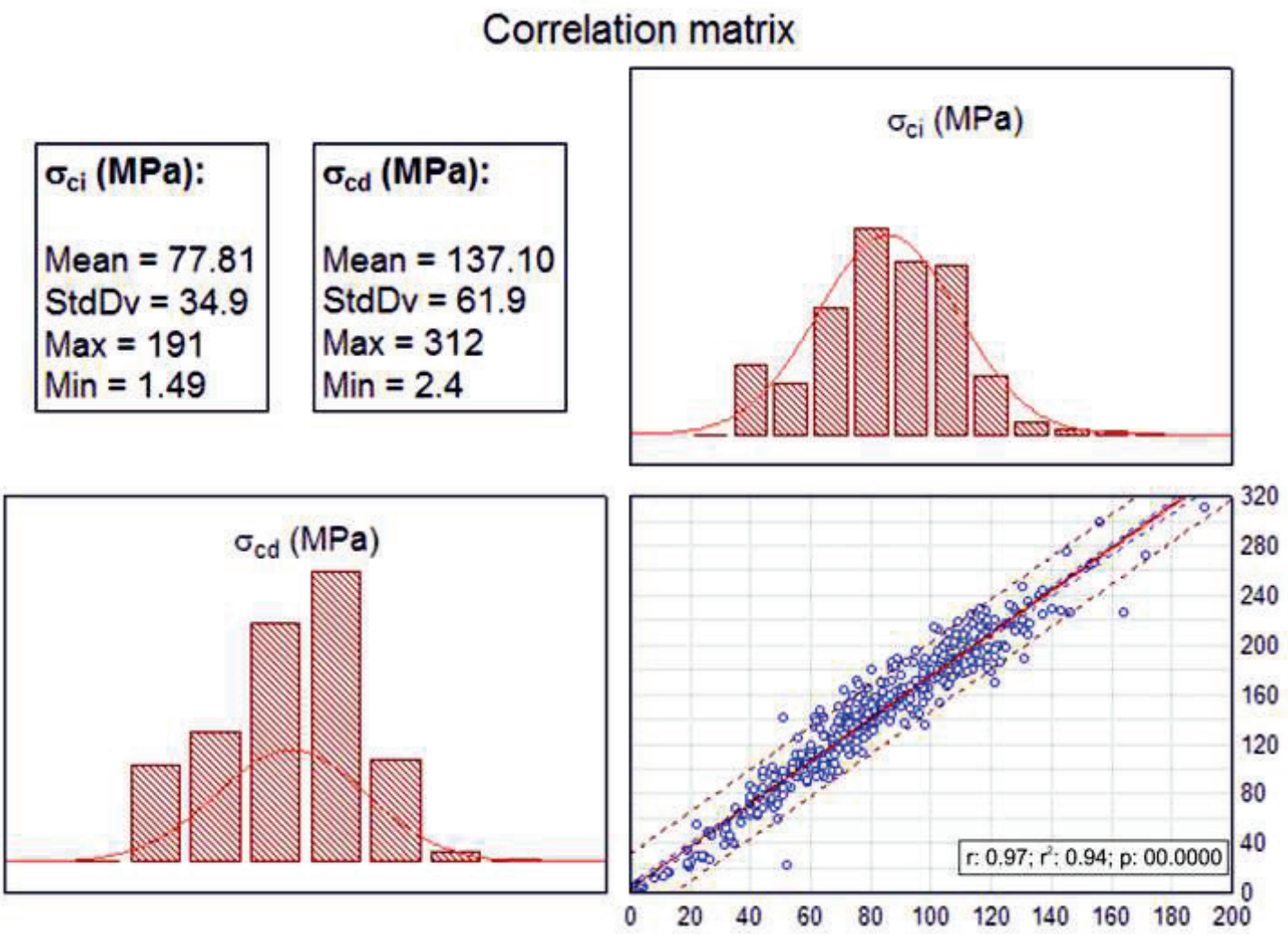

Figure10

Click here to download Figure Fig 10..tif

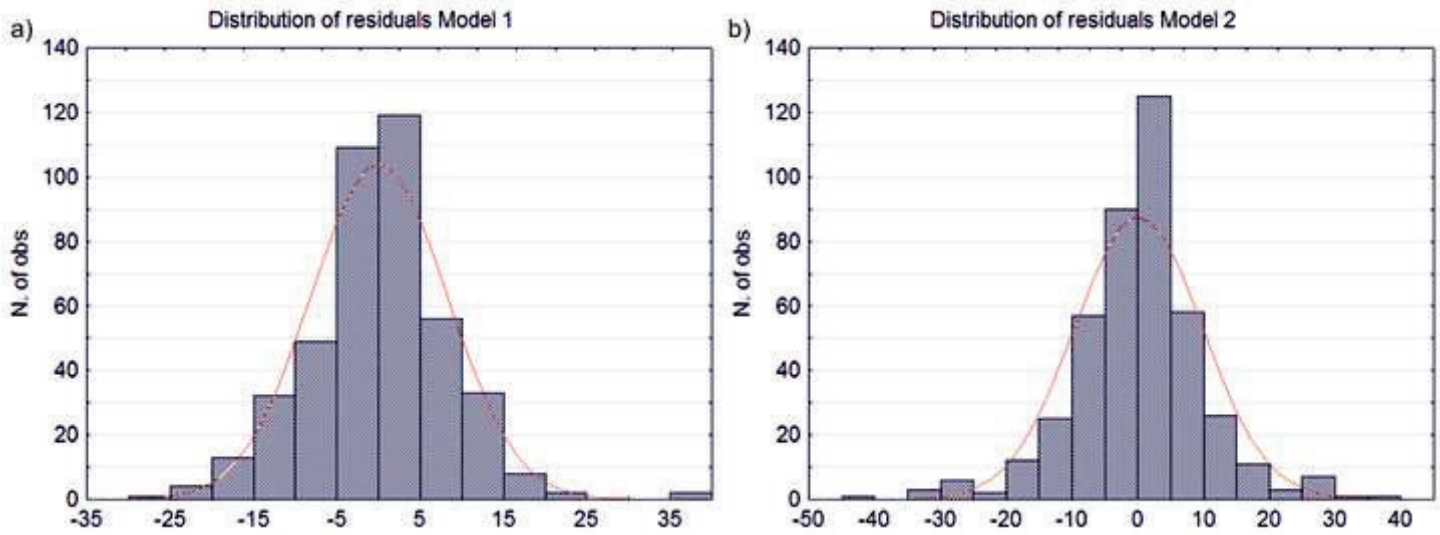

Figure11

Click here to download Figure Fig. 11.tif

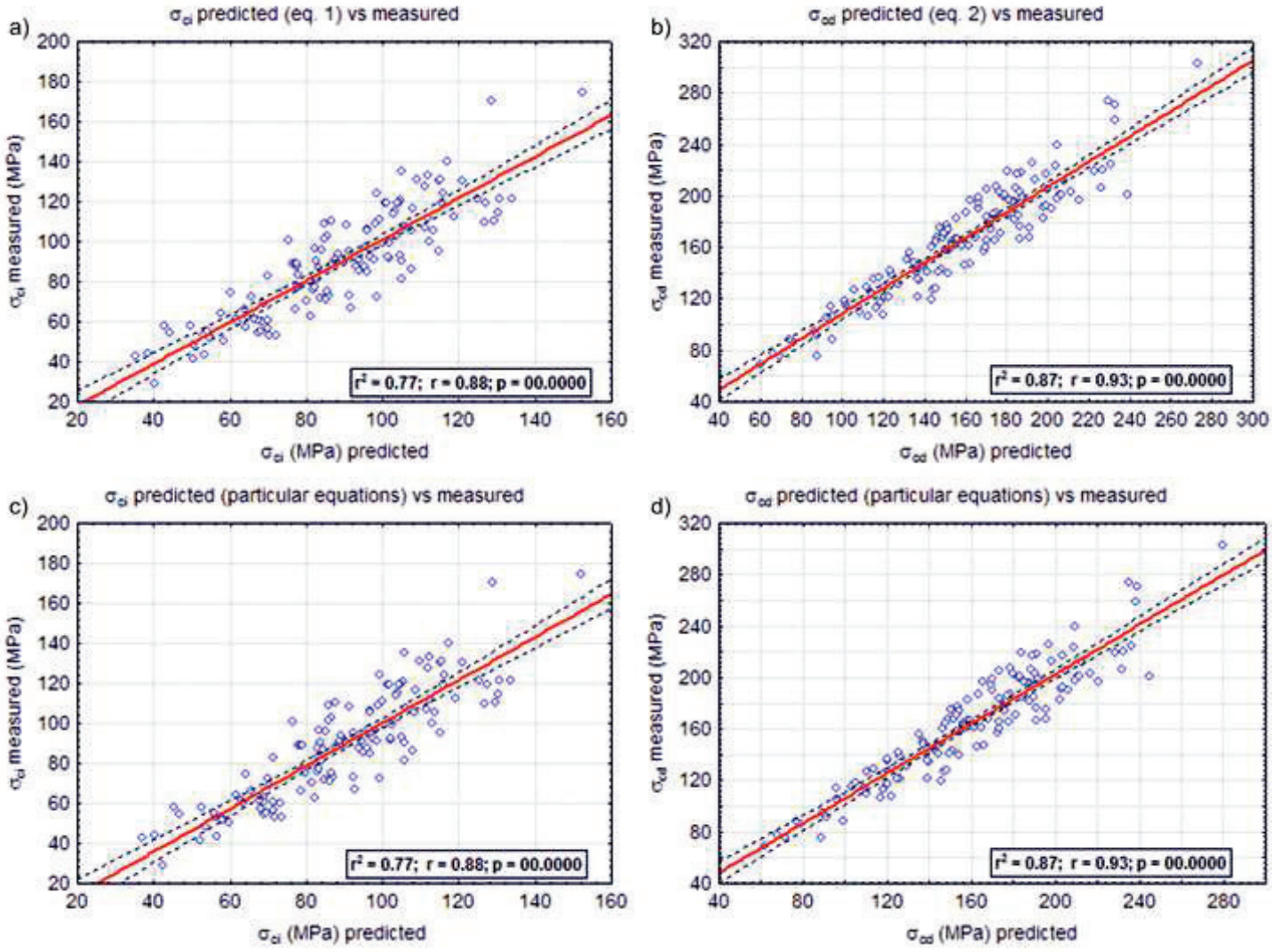

Figure12

Click here to download Figure Fig. 12.tif

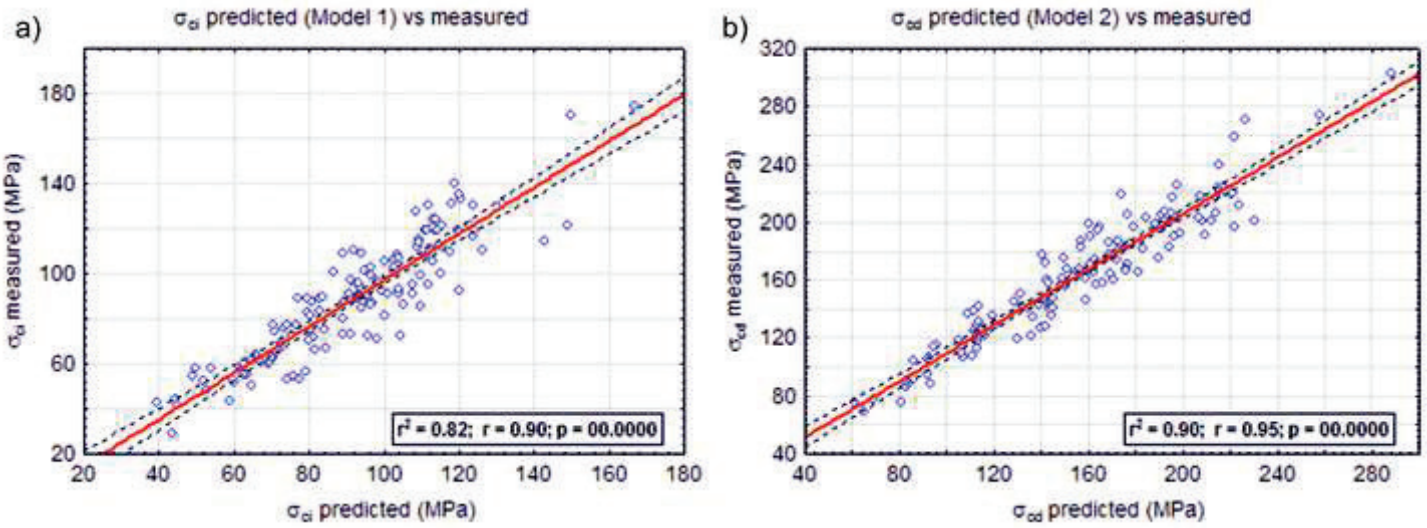

Table1

Table 1 Summary of the available intact rock data found in the literature including the number of specimens

Data sources	Rock type	n. of specimens	Available parameters				
			σ_{ucs}	σ_{ci}	σ_{cd}	E_{t50}	ν_{t50}
Amann et al. (2011)	Clay shale	19	X	X	X	X	X
Brace et al. (1966)	Sandstone	1	X	X	X		
Klein and Reuschlé (2004)	Sandstone	4	X	X			
Palchik and Hatzor (2002)	Limestone	12	X		X	X	X
Palchik and Hatzor (2002)	Dolomite	8	X		X	X	X
Gatelier et al. (2002)	Sandstone	7	X	X	X		
Ranjith et al. (2010)	Black coal	6	X	X	X		
Nicksiar (2013)	Argillaceous limestone	18	X	X	X	X	X
Nicksiar (2013)	Calcareous shale	4	X	X	X	X	X
Nicksiar (2013)	Shale	6	X	X	X	X	X
Liang et al. (2011)	Rock Salt	8	X		X	X	X
Cai (2010)	Quartzite	1	X	X			
Cai (2010)	Amphibolite	1	X	X			
Chang and Lee (2004)	Marble	1	X	X	X	X	X
Nicksiar (2013)	Amphibolite	4	X	X	X	X	X
Nicksiar (2013)	Meta-granite	32	X	X	X	X	X
Nicksiar (2013)	Micagneiss	51	X	X	X	X	X
Heikkilä and Hakala (1998a)	Tonalite gneiss	10	X	X	X	X	X
Andersson et al. (2009)	Diorite	7	X	X	X	X	X
Nicksiar and Martin (2012)	Diorite	10	X	X	X	X	X
Cai (2010)	Sulphide	10	X	X			
Cai (2010)	Peridotite	2	X	X			
Cai (2010)	Pegmatite	1	X	X			
Martin (1993)	Granite	3	X	X	X		
Fonseka et al. (1985)	Dolerite	1	X	X			
Chang and Lee (2004)	Granite	1	X	X	X	X	X
Lin et al. (2009)	Porphyritic monzonitic granite	4	X		X		
Nicksiar (2013)	Pegmatite	12	X	X	X	X	X
Nicksiar (2013)	Granodiorite	24	X	X	X	X	X
Nicksiar (2013)	Tonalite	9	X	X	X	X	X
Nicksiar (2013)	Granite	106	X	X	X	X	X
Nicksiar (2013)	Monzodiorite	32	X	X	X	X	X
Nicksiar (2013)	Diorite	17	X	X	X	X	X
Nicksiar (2013)	Rhyolite	5	X	X	X	X	X
Eloranta and Hakala (1998)	Porphyritic granodiorite	10	X	X	X	X	X
Eloranta and Hakala (1999a-b)	Granite	20	X	X	X	X	X
Heikkilä and Hakala (1998b)	Granite	10	X	X	X	X	X
Takarly et al. (2008)	Granite	6	X	X	X		

Table2

Table 2 Summary of the tested specimens for each rock type and main mineralogical features (data from Pepe et al. 2015, 2016, 2017).

Rock type	Specimens	Quartz	K-feldspar	Plagioclase	Hornblende	Biotite	Calcite	Muscovite
Meta-leucogranite	20	*	*	*	*	*	-	-
Meta-granite	31	*	*	*	*	*	-	-
Meta-syenogranite	9	*	*	*	-	*	-	-
Meta-granodiorite	31	*	*	*	*	*	-	-
Meta-monzonite	21	*	*	*	*	-	-	-
Limestone	20	*	-	-	-	-	*	*

Table3

Table 3 Summary of the main statistical information on the experimental results (CV coefficient of variation)

	Metamorphic rocks						Sedimentary rocks					
	σ_{ucs} (MPa)	σ_{ci} (MPa)	σ_{cd} (MPa)	E_{t50} (GPa)	σ_{ci}/σ_{ucs}	σ_{cd}/σ_{ucs}	σ_{ucs} (MPa)	σ_{ci} (MPa)	σ_{cd} (MPa)	E_{t50} (GPa)	σ_{ci}/σ_{ucs}	σ_{cd}/σ_{ucs}
Mean	206.8	95.1	175.1	59.9	0.46	0.85	121.4	58.7	108.3	41.0	0.49	0.90
St.Dev.	42.7	24.7	38.1	8.2	0.07	0.08	28.6	14.6	24.6	13.5	0.08	0.06
CV (%)	20.6	26.0	21.8	13.7	15.2	9.4	23.5	24.9	22.7	33.0	16.3	6.7

Table4

Table 4 Equations and r^2 of the statistical correlations with E_{t50} and ν_{t50}.

Correlation	**Equation**	**r^2**
E_{t50} vs σ_{ucs}	E_{t50} (MPa) = 23446.91 + 228.73 σ_{ucs}	0.61
E_{t50} vs σ_{ci}	E_{t50} (MPa) = 29038.29 + 440.82 σ_{ci}	0.55
E_{t50} vs σ_{cd}	E_{t50} (MPa) = 24331.88 + 273.85 σ_{cd}	0.60
ν_{t50} vs σ_{ucs}	ν_{t50} = 0.235 - 0.000031 σ_{ucs}	0.00
ν_{t50} vs σ_{ci}	ν_{t50} = 0.23 - 0.000065 σ_{ci}	0.00
ν_{t50} vs σ_{cd}	ν_{t50} = 0.237 - 0.000054 σ_{cd}	0.00